Interatomic potentials for atomic scale modeling of metal–matrix ceramic particle reinforced nanocomposites

A.M. Dongare [a], L.V. Zhigilei [b], A.M. Rajendran [c], B. LaMattina [d],*

[a] Department of Materials Science and Engineering, North Carolina State University, Raleigh, NC, USA
[b] Department of Materials Science and Engineering, University of Virginia, Charlottesville, VA, USA
[c] Department of Mechanical Engineering, University of Mississippi, Olemiss, MS, USA
[d] U.S. Army Research Office, Research Triangle Park, Raleigh, NC, USA

ARTICLE INFO

ABSTRACT

Functionally graded particle reinforced metal–matrix nanocomposite materials show significant promise for use in protective structures due to their high strengths, stiffness, failure resistance, and the ability to mitigate damage during ballistic impact. Further improvement of the performance of these materials requires fine-tuning of the nanostructure which, in turn, necessitates a clear fundamental understanding of the deformation and failure mechanisms under conditions of dynamic loading. While the molecular dynamics simulation technique is an excellent tool for investigation of the mechanisms of plastic deformation and failure of the particle reinforced metal–matrix nanocomposites at the atomic scale, the predictive power of the technique relies on an accurate description of the interatomic interactions. This paper provides a brief review of a recently developed class of interatomic potentials capable of the computationally efficient description of multi-component systems composed of metals, Si, Ge, and C. The potentials are based on reformulation of the Embedded Atom Method (EAM) potential for metals and two empirical potentials commonly used for covalently bonded materials, Stillinger–Weber (SW) and Tersoff, in a compatible functional form. The description of the angular dependence of interatomic interactions in the covalent materials is incorporated into the framework of the EAM potential and, therefore, the new class of potentials is dubbed Angular-dependent EAM (A-EAM) potentials. The A-EAM potentials retain all the properties of the pure components as predicted by the original SW, Tersoff, and EAM potentials, thus eliminating the need for extensive testing and limiting the scope of the potential parameterization to only the cross-interaction between the components. The performance of the A-EAM potentials is illustrated for the Au–Si system, with good agreement with experimental data obtained for the enthalpy of mixing in the Au–Si liquid alloy and the Au–Si phase diagram. The A-EAM potentials are suitable for large-scale atomistic simulations of metal–Si/Ge/C/SiC systems, such as the ones required for investigation of the dynamic response of nanocomposite materials to a ballistic/blast impact.

Published by Elsevier Ltd.

1. Introduction

One of the long-standing problems in materials research has been the development and improvement of materials capable of withstanding ballistic/blast impact. These materials have often been referred to as blast and penetration resistant materials (BPRMs). Better materials lead to better resistance and, in turn, greater survivability. In addition to overall structural stiffness and strength, BPRMs require the ability to mitigate damage and provide ways to dissipate impact/blast energy. Metals have proven to be cost effective, high performing materials for protective structures, particularly the ones with high impact strengths. Another parameter, important to penetration resistance, is ductility. An emerging class of materials for protective structures is functionally graded particle reinforced metal–matrix nanocomposites (MMnC) designed with compositional/structural gradients introduced through the variation of the concentration of the reinforcing ceramic particles (SiC, Al_2O_3, etc.) in the matrix [1,2]. Apart from their high strength, stiffness, and wear resistance, these nanocomposites have the ability to mitigate damage due to the spatial optimization of their properties. The trade-offs between the strength and ductility, observed in traditional metallic material systems, may not be applicable in these nanocomposites, leaving open the possibility of unprecedented performance improvements. The design and optimization of BPRM nanocomposite materials can be significantly accelerated by improvements in the understanding of the deformation and failure mechanisms under conditions of ballistic impact. Defense related loading conditions can result in impact velocities of a 1–2 km/s and peak strain rates of the order of

---

$10^5 - 10^6$ s^{-1} [3]. The mechanisms responsible for plastic deformation and failure of MMnC are complex and are affected by multiple factors, such as the distribution and location/size of the reinforcing particles, grain size in the metal–matrix, characteristics of the interfaces between the particles and matrix grains, as well as the loading conditions [4].

While there has been significant progress in the understanding the mechanisms of the plastic deformation in MMnC under quasi-static loading conditions, the material behavior at high strain rates is still at a stage of the initial exploration. The lack of detailed information on the response of the nanocomposite materials to the fast dynamic loading is related to the small time scales involved and the heterogeneous nature of these materials, which make it difficult to identify and characterize the elementary processes responsible for plastic deformation and failure using experiments alone. The molecular dynamics (MD) simulation technique has a potential of providing the atomic level structural information on the deformation mechanisms at high strain rates [5] and may be instrumental in physical interpretation of experimental observations. MD simulations of plastic deformation are typically carried out at strain rates $\geqslant 10^7$ s^{-1}. While these strain rates are higher than conventional strain rates in ballistic impact experiments, the current state-of-art simulations boast up to 350 billion atoms of copper corresponding to 1.56 μm size systems [6], as well as investigations of shock-induced phase transformations in multi-million atom samples [7]. With the increasing availability of computing resources, it should be possible to model deformation of systems comprising of many billions of atoms at realistic strain rates in the near future. Although the capabilities of MD method for investigations of mechanical behavior and properties of real materials are very promising, its ability to provide reliable quantitative information is, in a big part, defined by the availability of accurate and computationally efficient interatomic potentials.

Over the last several decades, a broad variety of empirical and semi-empirical potentials have been suggested in literature. For many of the potentials, however, the verification of their predictive power has been limited to relatively narrow domains of physical conditions, directly relevant to their applications in the initial studies. As a result, out of the vast number of potentials developed, only a relatively small fraction has been thoroughly tested and found to exhibit a combination of transferability, computational efficiency, and simplicity of implementation that ensures their broad use by many research groups. In particular, the Embedded Atom Method (EAM) [8–11] has provided the framework for a group of potentials that are used in the majority of current simulations of metals and metallic alloys. Popular potentials for covalently bonded systems include Stillinger–Weber (SW) potential [12,13] for Si and Ge, Tersoff potential [14,15] for Si and C, as well as Brenner potential [16,17] for hydrocarbon systems. The extension of the empirical potentials to alloys consisting of components with the same type of interatomic bonding (and described by the same type of interatomic potential) is relatively straightforward, with several alloy models (schemes for the description of cross-interactions between the components) developed for metals [11,18–21] and covalent systems [22,23]. The design of interatomic potentials capable of an adequate description of multi-component systems with mixed types of atomic bonding, however, is a more challenging task that has to be addressed to enable atomic scale modeling of a range of practically important systems. Computationally efficient and accurate description of systems with mixed metallic–covalent bonding, in particular, is highly desirable for investigation of the mechanical properties of metal–matrix nanocomposites reinforced by ceramic nanoparticles.

The Modified Embedded Atom Method (MEAM) potential [24] by Baskes includes parameterization for many cubic metals, as well as Si, Ge, C, H, N, and O. The potential, therefore, can be adopted for modeling of systems with mixed type of bonding, such as Mo–Si [25], Au–Si [26], and Au–Si–O [27]. A many-body angular screening function, used as a cutoff mechanism in MEAM, however, makes this potential to be computationally expensive. Moreover, the properties of both pure components and mixtures predicted by the MEAM potential have to be verified for each system of interest. An adjustment of the parameters of the MEAM potential, therefore, is often required in order to achieve an adequate description of the pure components [28]. Several potentials have been suggested for modeling of complex systems such as SiO$_2$ [29,30], SiC [31], and Alumina [32], with the charge transfer between the components explicitly incorporated into the models. The applicability of these potentials to study the pure elements and/or their interfaces with metallic systems has not been addressed.

An attractive alternative to the design of new alloy potentials with original functional forms can be provided by combination of well-established and thoroughly tested potentials developed for pure components within a unified approach. Despite the differences between the functional forms and underlying physical arguments used in the description of interatomic bonding in metallic and covalent systems, there has been a number of works suggesting the feasibility of the unified approach. In particular, a description of Pt–C system with an analytical potential that, for pure components, reduces to the bond-order Brenner potential for C and an EAM-like potential for Pt has been discussed by Albe et al. [33]. The connections between the EAM formalism and the bond-order scheme of the Tersoff potential have been discussed by Brenner [34], whereas the relationship between the SW and MEAM potentials has been discussed by Thijsse [35], who shows that the two potentials can be reformulated into compatible functional forms.

In this paper, we discuss the basic ideas and the functional form of a newly developed class of Angular-dependent EAM (A-EAM) potentials [36,37]. The A-EAM potentials incorporate a description of the angular dependence of interatomic interactions into the general framework of the EAM potential, making them compatible with the SW and Tersoff potentials. The A-EAM potentials retain all the properties of the pure components as predicted by the original SW, Tersoff, and EAM potentials, thus eliminating the need for extensive testing and limiting the extent of the parameterization needed. The reformulation of the EAM, SW, and Tersoff potentials leading to the development of the unified A-EAM potentials is described in Section 2. The ability of the A-EAM potentials to provide an adequate description of binary systems with mixed type of bonding is illustrated in Section 3, where some of the thermodynamic properties of the Au–Si alloy represented by an A-EAM potential are discussed.

2. The Angular-dependent Embedded Atom Method

A unified alloy potentials based on a reformulation of the EAM, SW, and Tersoff potentials in a compatible functional form are discussed in this section. A reformulation of the conventional EAM potential into a general A-EAM form that includes three-body terms in the expression for the total electron density function is presented first, followed by a description of two approaches developed for incorporation of the angular dependence compatible with either SW or Tersoff potentials.

2.1. EAM potential with three-body terms in the electron density function

In the EAM potentials, the energy of an atom is expressed as

$$E_i = \frac{1}{2} \sum_{j \neq i} \phi_{ij}(r_{ij}) + F_i(\rho_i), \tag{1}$$

where r_{ij} is the distance between atoms i and j, $\phi_{ij}(r_{ij})$ is the pair energy term defined as a function of the interatomic distance, $F_i(\rho_i)$ is the embedding energy term defined as a function of the electron density ρ_i at the position of atom i, and the summation is over all atoms interacting with atom i. The electron density ρ_i is calculated as a sum of the partial electron density contributions from the neighboring atoms,

$$\rho_i = \sum_{j \neq i} f_j(r_{ij}), \tag{2}$$

where $f_j(r_{ij})$ is the partial electron density contribution from atom j at the location of atom i. Since only interatomic distances r_{ij} are needed to calculate the energy and forces in the system, the EAM calculations are nearly as simple and computationally efficient as the ones with pair potentials. The lack of explicit three-body terms, however, makes the conventional EAM to be inappropriate for covalently bonded materials.

To make connections to SW or Tersoff potentials and to allow for the introduction of an angular dependence of the interatomic interactions, the linear sum of partial electron density contributions in Eq. (2) can be expressed through the sum of products of partial electron densities,

$$\rho_i = \left(\left[\sum_{j \neq i} f_j(r_{ij}) \right]^2 \right)^{1/2} = \left(\sum_{k \neq i} \sum_{j \neq i} f_j(r_{ij}) f_k(r_{ik}) \right)^{1/2}. \tag{3}$$

The sum in the right part of the above equation includes two-body terms with identical pairs of atoms ($j = k$) and three-body terms ($j \neq k$) that can be separated from each other [35]. The three-body terms can be written in the form of a sum over unique triplets of atoms (i, j, k):

$$\rho_i = \left\{ \sum_{j \neq i} [f_j(r_{ij})]^2 + 2 \sum_{j,k \in T_i} f_j(r_{ij}) f_k(r_{ik}) \right\}^{1/2}, \tag{4}$$

where in the first (two-body) term under the square root the summation is over all atoms interacting with atom i, and in the second (three-body) term the summation is over all pairs of atoms j and k that form unique triplets with atom i. This formulation includes an explicit dependence on triplets of neighboring atoms and, as shown in Section 2.2, allows for incorporation of an angular dependence of the interatomic interactions in a form compatible with Stillinger–Weber potential. Alternatively, the three-body terms can be written in a form of the "bond order" dependence:

$$\rho_i = \left\{ \sum_{j \neq i} [f_j(r_{ij})]^2 + \sum_{j \neq i} f_j(r_{ij}) \sum_{k \neq i,j} f_k(r_{ik}) \right\}^{1/2}. \tag{5}$$

This formulation includes a bond order dependence and, as shown in Section 2.3, allows for the incorporation of an angular dependence of the interatomic interactions in a form compatible with Tersoff potential.

2.2. Angular-dependent EAM compatible with SW potential (metal–Si/Ge systems)

The energy of an atom in a system described by SW potential is defined as [12]

$$E_i = \frac{1}{2} \sum_{j \neq i} U_2(r_{ij}) + \sum_{j,k \in T_i} U_3(\vec{r}_i, \vec{r}_j, \vec{r}_k). \tag{6}$$

The potential consists of a two-body (U_2) and three-body (U_3) terms, with the summation of the three-body terms being over all atom pairs j and k that form unique triplets with atom i. The two-body term has a Lennard–Jones form terminated at a distance r_c by a cutoff function:

$$U_2(r_{ij}) = A \left[B \left(\frac{r_{ij}}{\sigma} \right)^{-p} - \left(\frac{r_{ij}}{\sigma} \right)^{-q} \right] \exp \left[\frac{\sigma}{r_{ij} - r_c} \right]. \tag{7}$$

The three-body term is defined as

$$U_3(\vec{r}_i, \vec{r}_j, \vec{r}_k) = \lambda \varepsilon \exp \left[\frac{\gamma \sigma}{r_{ij} - r_c} + \frac{\gamma \sigma}{r_{ik} - r_c} \right] (\cos \theta_{jik} + 1/3)^2$$
$$\text{for} \quad r_{ij} < r_c, r_{ik} < r_c, \tag{8}$$

were θ_{jik} is an angle between vectors $\vec{r}_{ij}$ and $\vec{r}_{ik}$ originating from atom i and directed to atoms j and k. The parameters A, B, p, q, λ, σ, ε, r_c, and γ are adjustable parameters that are chosen to reproduce the properties of crystalline, liquid, and amorphous phases, as well as surface structures for Si or Ge [12,13,38,39].

The sum of the three-body terms in Eq. (6) can be rewritten in a form of embedding energy,

$$F_i(\rho_i) = \sum_{j,k \in T_i} U_3(\vec{r}_i, \vec{r}_j, \vec{r}_k) = \frac{\lambda \varepsilon}{2(f_e)^2} \rho_i^2, \tag{9}$$

where the electron density and partial electron density contributions are defined as

$$\rho_i = \left(2 \sum_{j,k \subset T} f_{ij}(r_{ij}) f_{ik}(r_{ik}) (\cos \theta_{jik} + 1/3)^2 \right)^{1/2}, \tag{10}$$

$$f_{ij}(r_{ij}) = f_e \exp \left(\frac{\gamma \sigma}{r_{ij} - r_c} \right). \tag{11}$$

Note that in the expression for the electron density given by Eq. (10), the partial electron density contributions are defined by the types of the pairs of atoms forming the bond, $f_{ij}(r_{ij})$, rather than the type of the neighboring atom, $f_j(r_{ij})$, as in the original EAM, Eq. (2). As discussed in Section 3, this gives a greater flexibility in the parameterization of the metal–covalent cross-interactions. Using the reformulation of the three-body terms of the SW potential in the functional form of the EAM embedding function, Eq. (9), and taking the pair energy term of the EAM potential in the form of the two-body term of the SW potential, $\phi_{ij}(r_{ij}) = U_2(r_{ij})$, the SW potential can be written in the form of the EAM potential, Eq. (1). For an alloy system containing both metal and Si/Ge atoms, a combined potential that reduces to the conventional SW and EAM potentials for pure components can be then formulated as

$$E_i = \frac{1}{2} \sum_{j \neq i} \phi_{ij}(r_{ij}) + F_i \left[\left\{ (1 - \delta_i) \sum_{j \neq i} (f_{ij}(r_{ij}))^2 \right. \right.$$
$$\left. \left. + 2 \sum_{j,k \subset T_i} f_{ij}(r_{ij}) f_{ik}(r_{ik}) (\cos \theta_{jik} + 1/3)^{c_i} \right\}^{1/2} \right]. \tag{12}$$

Two parameters, δ_i and c_i, are added to ensure that the combined potential given by Eq. (12) reduces to the conventional EAM potential for pure metals and to the original SW potential for pure silicon/germanium. For metals, $\delta_i = c_i = 0$ excludes the angular dependence and retains only the radial contributions to the electron density, thus, reducing to the original EAM potential, Eqs. (1) and (4). For Si/Ge, $\delta_i = 1$ and $c_i = 2$ reduces the electron density function into the three-body function of the SW potential, Eq. (10), that retains the angular dependence. The functional form and parameters of the embedding energy functions, $F_i(\rho_i)$, as well as the pair energy and partial electron density functions for the interactions between atoms of the same type are directly defined by the original EAM and SW potentials and do not need to be adjusted in the alloy potential. The adjustable parameter f_e in Eqs. (9) and (11) is chosen based on the characteristics of the EAM potential for the metal component [37]. This parameter, once fixed, is not used in further fitting of the cross-interactions in the potential. The fitting of the alloy

potential, therefore, is limited to finding the optimum parameters for the pair energy term, $\phi_{ij}(r_{ij})$, and the partial electron density contributions, $f_{ij}(r_{ij})$, for cross-interactions between atoms of different type. Parameterization of the potential for Au–Si and Au–Ge systems, based on the results of Density Functional Theory (DFT) calculations performed for several representative Au–Si/Ge bulk structures and small clusters, is reported in Ref. [37]. The ability of the potential for Au–Si to reproduce some of the thermodynamic properties of the Au–Si alloy is briefly reviewed in Section 3.

The angular dependence of interatomic interactions is incorporated into the alloy potential given by Eq. (12) in a form that is compatible with SW potential. This potential is therefore referred to as the SW formulation of the A-EAM potential, or A-EAM (SW). An alternative approach for incorporation of the angular dependence, compatible with Tersoff potential, is discussed below.

2.3. Angular-dependent EAM compatible with Tersoff potential (metal–Si/Ge/C/SiC systems)

The Tersoff potential is based on the concept of *bond order* which implies that the strength of a bond between two atoms is not constant, but depends on the local environment [14]. The energy of an atom in a system described by Tersoff potential [14,23] is defined as half of the sum of bond energies V_{ij},

$$E_i = 1/2 \sum_{j \neq i} V_{ij}, \quad \text{where} \quad V_{ij} = f_C(r_{ij})[f_R(r_{ij}) - b_{ij} f_A(r_{ij})]. \tag{13}$$

Here, $f_R(r_{ij})$ and $f_A(r_{ij})$ correspond to the repulsive and attractive parts of the potential, $f_C(r_{ij})$ is the cutoff function that limits the range of the interatomic interactions, and b_{ij} is the bond order term which depends on the local environment of atoms i and j. The functional form of these terms is given as

$$f_R(r_{ij}) = A \exp(-\lambda_1 r_{ij}), \tag{14}$$

$$f_A(r_{ij}) = B \exp(-\lambda_2 r_{ij}), \tag{15}$$

$$f_C(r_{ij}) = \begin{cases} 1 & \text{for} \quad 0 < r_{ij} < R_C \\ 1/2 + 1/2 \cos\left[\pi\left(\frac{r_{ij} - R_C}{S_C - R_C}\right)\right] & \text{for} \quad R_C < r_{ij} < S_C, \\ 0 & \text{for} \quad r_{ij} > S_C \end{cases} \tag{16}$$

$$b_{ij} = \left[1 + \beta^n \left(\sum_{k \neq i,j} f_C(r_{ik}) g(\theta_{jik})\right)^n\right]^{-1/2n}, \tag{17}$$

where the function defining the angular dependence of the bond order term is given as

$$g(\theta_{jik}) = 1 + \frac{c^2}{d^2} - \frac{c^2}{[d^2 + (h - \cos\theta_{jik})^2]}. \tag{18}$$

The expression for the bond energy in Eq. (13) can be rearranged [40] to have explicit two-body and three-body terms, $V_{ij} = V_2 + V_3$, where

$$V_2 = f_C(r_{ij})[f_R(r_{ij}) - f_A(r_{ij})], \tag{19}$$

$$V_3 = f_A(r_{ij}) f_C(r_{ij})[1 - b_{ij}]. \tag{20}$$

To rewrite the Tersoff potential in the form compatible with the EAM potential given by Eq. (1), the pair energy term, the embedding function, and the electron density function can be formulated as follows:

$$\phi_{ij}(r_{ij}) = V_2 = f_C(r_{ij})[f_R(r_{ij}) - f_A(r_{ij})], \tag{21}$$

$$F_i[\rho_i] = \frac{1}{2f_e}(\rho_i)^2, \tag{22}$$

$$\rho_i = \left(\sum_{j \neq i} V_3\right)^{1/2}$$
$$= \left\{\sum_{j \neq i} f_{ij}(r_{ij})\left\{1 - \left[1 + \beta^n \left(\sum_{k \neq i,j} f_C(r_{ik}) g(\theta_{jik})\right)^n\right]^{-1/2n}\right\}\right\}^{1/2}, \tag{23}$$

where the partial electron density function is defined as

$$f_{ij}(r_{ij}) = f_e f_A(r_{ij}) f_C(r_{ij}). \tag{24}$$

Using the similarity between the electron density function given by Eq. (23) and the one of a conventional EAM written in the bond order form in Eq. (5), the EAM and Tersoff potentials can be written in a single functional form given by Eq. (1), with the electron density function defined as

$$\rho_i = \left\{(1 - \delta_3) \sum_{j \neq i} (f_{ij}(r_{ij}))^2 \right.$$
$$\left. + \sum_{j \neq i} f_{ij}(r_{ij})\left\{\delta_1 + \delta_2\left[1 + t_\beta\left(\sum_{k \neq i,j} (f_{ik}(r_{ik}))^{\delta_4} [f_C(r_{ik}) g(\theta_{jik})]^{\delta_5}\right)^x\right]^y\right\}\right\}^{1/2}. \tag{25}$$

The eight parameters/switches of the alloy potential (δ_1, δ_2, δ_3, δ_4, δ_5, x, y, and t_β) are chosen based on the type of atom i, so that the electron density function reduces to Eq. (5) for a metal atom ($\delta_1 = -1$, $\delta_2 = 1$, $\delta_3 = 0$, $\delta_4 = 1$, $\delta_5 = 0$, $x = 1$, $y = 1$, $t_\beta = 1$) and to Eq. (23) for Si, Ge or C represented by Tersoff potential ($\delta_1 = 1$, $\delta_2 = -1$, $\delta_3 = 1$, $\delta_4 = 0$, $\delta_5 = 1$, $x = n$, $y = -1/2n$, $t_\beta = \beta^n$).

The angular dependence of interatomic interactions is incorporated into the alloy potential given by Eqs. (1) and (25) in a form that is compatible with Tersoff potential. Thus, this potential is referred to as the Tersoff formulation of the A-EAM potential, or A-EAM (T). Similarly to the A-EAM (SW) potential discussed above, in A-EAM (T) the embedding energy functions as well as the pair energy and partial electron density functions for the interactions between atoms of the same type are defined by the original EAM and Tersoff potentials. The adjustable parameter f_e in Eqs. (22) and (24) is chosen based on the characteristics of the EAM potential for the metal component. The pair energy term and the partial electron density contributions for cross-interactions between atoms of different type can be chosen by fitting the energies, structural characteristics, and/or thermodynamic parameters of various systems composed of atoms of different type to experimental data and/or results of *ab initio* calculations.

3. Thermodynamics of Au–Si alloy represented by the A-EAM (SW) potential

To illustrate the ability of the A-EAM potentials to reproduce the properties of materials with mixed metallic–covalent bonding, the results of the calculations of the phase diagram and the enthalpy of mixing in the liquid phase are briefly discussed in this Section for the A-EAM (SW) potential parameterized for Au–Si system. A detailed discussion of the functional form and parameters of the pair energy and partial electron density functions chosen for cross-interactions between atoms of different type, as well as the results of DFT calculations used in the parameterization of the potential, are given in Ref. [37]. Briefly, the combined A-EAM (SW) potential is based on the SW potential for Si [12] and Johnson's EAM potential for Au, taken in the form suggested in Ref. [20]. The advantage of this formulation of the EAM potential is in the

simplicity of the functional form and the availability of parameterizations for many metals, allowing for an easy implementation for a broad range of alloy systems.

The parameters for Si–Si and Au–Au interactions are defined by the original EAM and SW potentials, with corresponding plots of the embedding energy functions, the pair energy functions, and the partial electron density functions for Au and Si shown in Fig. 1 by the solid lines. The functional form and parameters of the pair energy functions and the electron density functions for cross-interactions between Si and Au atoms are selected based on the results of DFT calculations performed for several Au–Si bulk structures and small clusters. The plots of the pair energy function and the partial electron density function for cross-interactions are shown in Fig. 1 by the dashed lines for the set of parameters that provides a good representation of the results of the DFT calculations.

As apparent from Fig. 1c, the partial electron density contribution from Si to Au is larger than the one from Au to Si. Our initial attempt to use the same partial electron density contributions, $f_{ij}(r_{ij}) = f_{ji}(r_{ij})$, resulted in unsatisfactory representation of some of the material properties, particularly the experimental dependence of the enthalpy of mixing of the liquid alloy on the composition. The large difference in the partial electron density contributions from Au to Si and from Si to Au (Fig. 1c), can be related to the partial charge transfer from Si to Au predicted in DFT calculations [37,41]. This charge transfer can be attributed to higher electronegativity of Au as compared to Si, 2.54 vs. 1.90 in Pauling units. From the point of view of the performance of the A-EAM (SW) potential given by Eq. (12), the reduction in the electron density for a Si atom due to the presence of Au atoms in its neighborhood corresponds to the weakening of the strength of the angular interactions. On the other hand, the higher values of the partial electron density contribution from Si to Au, as compared to Au–Au interactions, imply that a Au atom has an increased electron density and, therefore, more repulsive interactions with the neighboring atoms, when it has Si atoms as its neighbors.

To test the thermodynamic properties of the Au–Si system as predicted by the A-EAM potential at finite temperatures, the values of the enthalpy of mixing of the liquid alloy and the equilibrium lines on the Au–Si phase diagram are calculated and compared with experimental data. The calculated and experimental dependences of the enthalpy of mixing on the composition of the liquid alloy are show for 1500 K in Fig. 2. Similar to the experimental data [42], the dependence predicted by the A-EAM (SW) potential [37] has an asymmetric shape, with minimum shifted toward the Au-rich alloys. The calculated dependence has a minimum of −9.88 kJ/mol at a concentration of 33 at.% Si, compared to the experimental dependence exhibiting a minimum of −8.23 kJ/mol at a composition of 24 at.% Si.

The equilibrium phase diagram predicted by the A-EAM (SW) potential for Au–Si system is shown in Fig. 3a. The calculation of the phase diagram is based on the values of the excess chemical potential difference between Au and Si, evaluated in a series of semi-grand canonical ensemble Monte Carlo simulations [43,44] performed for different temperatures and alloy compositions. The liquidus lines on the phase diagram are obtained by computing the Gibbs free energy of mixing for the liquid phase and the Gibbs free energies of solid phases at different temperatures, and then using the common tangent construction [37]. The Au–Si phase diagram predicted by the A-EAM (SW) potential is of the simple eutectic type, and matches relatively well the experimental phase diagram shown in Fig. 3b. The A-EAM (SW) potential predicts a eutectic temperature of 590 K, which is comparable to the experimental eutectic temperature of 636 K. The eutectic composition of 31 at.% Si, predicted by the A-EAM (SW) potential, however, exhibits a substantial deviation from the experimental value of 18.6 at.% Si. The deviation in the eutectic composition and the eu-
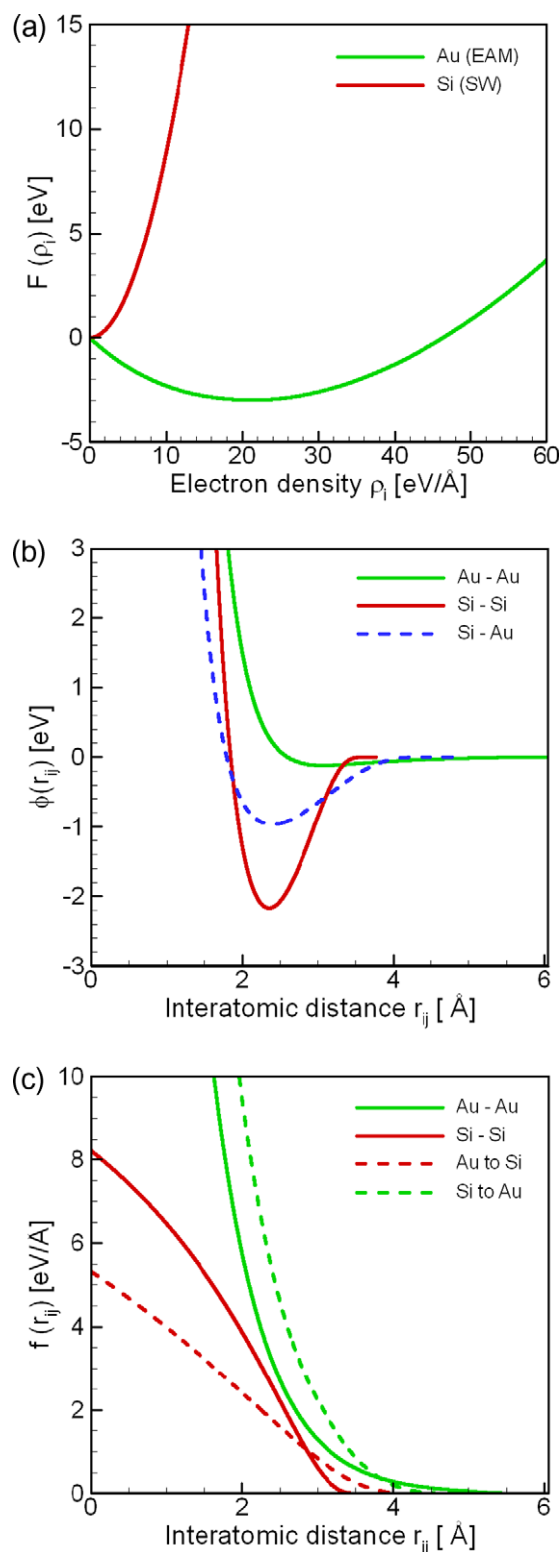

Fig. 1. Plots of (a) the embedding functions for EAM Au (green line) and SW Si (red line), (b) the pair potentials, and (c) the partial electron density contributions for the A-EAM (SW) potential for Au–Si system [37]. The red line corresponds to the Si–Si interaction, the green line corresponds to the Au–Au interaction. The dashed blue line in (b) corresponds to the cross Au–Si pair interaction. The dashed green curve and the dashed red curve in (c) represent the partial electron density contribution from Si to Au and Au to Si, respectively. (For interpretation of the references to color in this figure legend, the reader is referred to the web version of this article.)

tectic temperature can be attributed to the lower melting point of the EAM Au material (963 K [45] as compared to the experimental
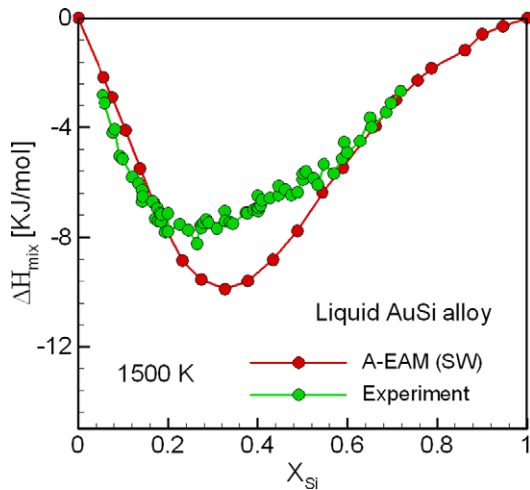
Fig. 2. Enthalpy of mixing of the liquid Au–Si alloy at 1500 K. The values predicted by the A-EAM (SW) potential are shown by red dots [37] and the experimental data [42] is shown by the green dots. (For interpretation of the references to color in this figure legend, the reader is referred to the web version of this article.)
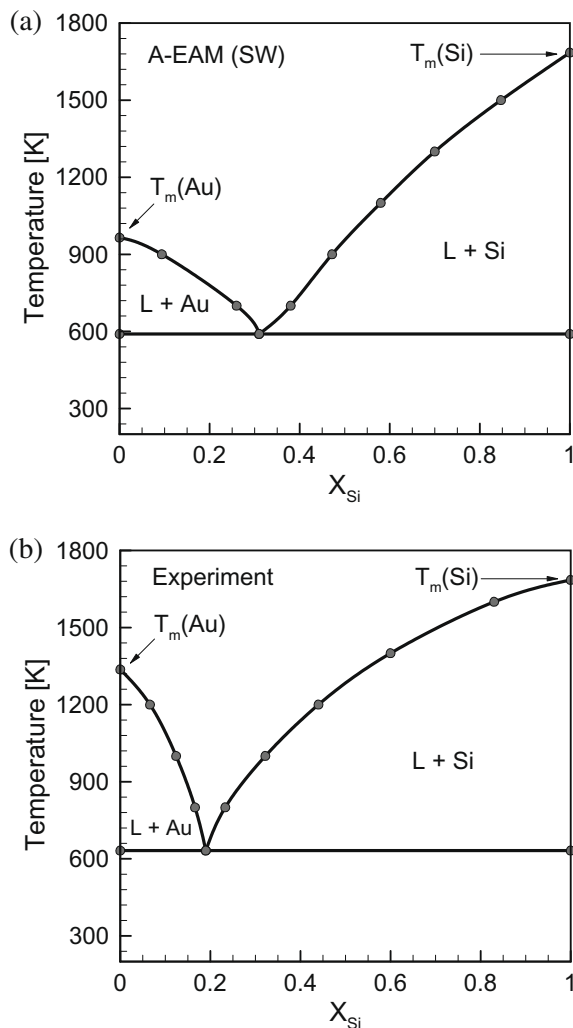

Fig. 3. Phase diagrams of the Au–Si alloy predicted by the A-EAM (SW) potential [37] (a) and obtained experimentally [42] (b). The eutectic temperatures and compositions are 590 K and 31 at.% Si in (a) and 636 K and 18.6 at.% Si in (b).

melting temperature of 1336 K [46]), as well as to the shift of the location of the minimum of the composition dependence of the enthalpy of mixing to higher values of Si concentration compared to the experimental data (Fig. 2). Thus, a more accurate fitting of the Au–Si cross-interaction to the enthalpy of mixing of the liquid alloy, along with improved melting properties of the EAM Au can be expected to result in a more accurate representation of the experimental Au–Si phase diagram by the A-EAM (SW) potential.

The application of the A-EAM potential to simulations of plastic deformation and fracture of particle reinforced metal–matrix nano-composite materials requires additional testing of a range of properties relevant to the mechanical behavior of the model material (such as characteristics of crystal defects and solid-state crystalline and disordered phases). The advantage of the multi-component A-EAM potentials discussed in this work, however, is that they inherit all the properties of pure components predicted by the corresponding potentials. The potentials for pure components (Stillinger–Weber, Tersoff, and EAM) have been extensively used and thoroughly tested, including for the properties relevant to the dynamic plastic deformation and fracture. The properties of the interfaces and mixed regions in the nanocomposite materials are defined by cross-parameterization of the combined potential, discussed in this work. While in this paper we did not test the cohesive strength of the interfaces directly, the negative values of the enthalpy of mixing and the eutectic type of the phase diagram indicate that the interfacial (mixed) part of the system have a weaker average cohesive strength as compared to the pure components. Moreover, a reasonable quantitative agreement in the calculated and experimental values of the enthalpy of mixing and the eutectic temperature suggests that the potential is appropriate for a semi-quantitative description of the interfaces in the nanocomposite materials.

4. Summary

A new class of interatomic potentials capable of a computationally efficient description of metal–covalent systems is reviewed in the context of the prospective applications for investigation of the dynamic response of metal–matrix ceramic particle reinforced nanocomposite materials to a ballistic impact. The proposed A-EAM framework is based on the combination of well-established and thoroughly tested potentials developed for pure components and, therefore, provides an attractive alternative to the design of new alloy potentials with original functional forms. The design of A-EAM potentials involves the reformulation of the electron density function of the conventional EAM potential to include three-body angular dependent interactions. The angular dependence is included through either an explicit dependence on triplets of neighboring atoms or a bond-order type of dependence, making it possible to combine the EAM potential for metals with Stillinger–Weber or Tersoff potentials used for covalently bonded materials. The complex effects related to the charge transfer in the mixed interactions can be accounted for in the potential by defining the partial electron density contributions based on the type of the pair of atoms forming a bond, rather than the types of individual atoms. The initial implementation of the A-EAM approach for Au–Si system demonstrates the ability of the potential to provide an adequate description of the structural and thermodynamic properties of the alloy at different temperatures and in the whole range of compositions. Thus, the A-EAM potentials show considerable promise for investigations of multi-component materials with mixed metallic–covalent bonding.

References

[1] Mortensen A, Suresh S. Functionally graded metals and metal–ceramic composites. Part 1: Processing. Int Mat Rev 1995;40:239–65.

[2] Suresh S, Mortensen A. Functional graded metals and metal–ceramic composites. Part 2: Thermomechanical behavior. Int Mat Rev 1997;42:85–116.

[3] Ramesh KT. High strain rate and impact testing. In: Sharpe WN, editor. Springer handbook of experimental solid mechanics. NY: Springer; 2008. p. 929–60.

[4] Li Y, Ramesh KT, Chin ESC. Plastic deformation and failure in A359 aluminum and an A359-SiCp MMC under quasistatic and high-strain-rate tension. J Compos Mater 2007;41:27–40.

[5] Brenner DW. Computer modeling of nanostructured materials. In: Koch CC, editor. Nanostructured materials: processing, properties, and applications. William Andrew Publishing; 2007. p. 293–328.

[6] Kadau K, Germann TC, Lomdahl PS. Molecular dynamics comes of age: 320 billion atom simulation on BlueGene/L. Int J Mod Phys C 2006;17:1755–61.

[7] Kadau K, Germann TC, Lomdahl PS, Holian BL. Microscopic view of structural phase transitions induced by shock waves. Science 2002;296:1681–4.

[8] Daw MS, Baskes MI. Embedded-atom method: derivation and application to impurities, surfaces, and other defects in metals. Phys Rev B 1984;29:6443–53.

[9] Foiles SM. Application of the embedded-atom method to liquid transition metals. Phys Rev B 1985;32:3409–15.

[10] Johnson RA. Analytic nearest-neighbor model for fcc metals. Phys Rev B 1988;37:3924–31.

[11] Voter AF. The embedded atom method. In: Westbrook JH, Fleischer RL, editors. Intermetallic compounds: principles and practice. New York: Wiley; 1995. p. 77–90.

[12] Stillinger FH, Weber TA. Computer simulation of local order in condensed phases of silicon. Phys Rev B 1985;31:5262–71.

[13] Ding K, Andersen H. Molecular-dynamics simulation of amorphous germanium. Phys Rev B 1986;34:6987–91.

[14] Tersoff J. New empirical approach for the structure and energy of covalent systems. Phys Rev B 1988;37:6991–7000.

[15] Tersoff J. Empirical interatomic potential for carbon, with applications to amorphous carbon. Phys Rev Lett 1988;61:2879–82.

[16] Brenner DW. Empirical potential for hydrocarbons for use in simulating the chemical vapor deposition of diamond films. Phys Rev B 1990;42:9458–71.

[17] Brenner DW, Shenderova OA, Harrison JA, Stuart SJ, Ni B, Sinnot SB. A second-generation reactive empirical bond order (REBO) potential energy expression for hydrocarbons. J Phys Condens Mat 2002;14:783–802.

[18] Foiles SM, Baskes MI, Daw MS. Embedded-atom-method functions for the fcc metals Cu, Ag, Au, Ni, Pd, Pt, and their alloys. Phys Rev B 1986;33:7983–91.

[19] Johnson RA. Alloy models with the embedded-atom method. Phys Rev B 1989;39:12554–9.

[20] Zhou XW, Wadley HNG, Johnson RA, Larson DJ, Tabat N, Cerezo A, et al. Atomic scale structure of sputtered metal multilayers. Acta Mater 2001;49:4005–15.

[21] Rafii-Tabar H, Sutton AP. Long-range Finnis–Sinclair potentials for f.c.c. metallic alloys. Philos Mag Lett 1991;63:217–24.

[22] Laradji M, Landau DP, Dünweg B. Structural properties of $Si_{1-x}Ge_x$ alloys: a Monte Carlo simulation with the Stillinger–Weber potential. Phys Rev B 1995;51:4894–902.

[23] Tersoff J. Modeling solid-state chemistry: interatomic potentials for multicomponent systems. Phys Rev B 1989;39:5566–8.

[24] Baskes MI. Modified embedded-atom potentials for cubic materials and impurities. Phys Rev B 1992;46:2727–42.

[25] Baskes MI. Atomic potentials for the molybdenum–silicon system. Mater Sci Eng A 1999;261:165–8.

[26] Kuo C-L, Clancy P. MEAM molecular dynamics study of a gold thin film on a silicon substrate. Surf Sci 2004;551:39–58.

[27] Kuo C-L, Clancy P. Development of atomistic MEAM potentials for the silicon–oxygen–gold ternary system. Model Simul Mater Sci Eng 2005;13:1309–29.

[28] Thijsse BJ. Silicon potentials under (ion) attack: towards a new MEAM model. Nucl Instrum Meth B 2005;228:198–211.

[29] Yu J, Phillpot SR, Sinnott SB. Interatomic potential for the structure and energetics of tetrahedrally coordinated silica polymorphs. Phys Rev B 2007;75:233203.

[30] Vashishta P, Kalia RK, Rino JP. Interaction potential for SiO_2: a molecular-dynamics study of structural correlations. Phys Rev B 1990;41:12197–209.

[31] Vashishta P, Kalia RK, Nakano A, Rino JP. Interaction potential for silicon carbide: a molecular dynamics study of elastic constants and vibrational density of states for crystalline and amorphous silicon carbide. J Appl Phys 2007;101:103515.

[32] Vashishta P, Kalia RK, Nakano A, Rino JP. Interaction potentials for alumina and molecular dynamics simulations of amorphous and liquid alumina. J Appl Phys 2008;103:083504.

[33] Albe K, Nordlund K, Averback RS. Modeling the metal–semiconductor interaction: analytical bond-order potential for platinum–carbon. Phys Rev B 2002;65:195124.

[34] Brenner DW. Relationship between the embedded-atom method and Tersoff potentials. Phys Rev Lett 1989;63:1022.

[35] Thijsse BJ. Relationship between the modified embedded-atom method and Stillinger–Weber potentials in calculating the structure of silicon. Phys Rev B 2002;65:195207.

[36] Dongare AM, Zhigilei LV. In: Proceedings of the international conference on computational and experimental engineering and sciences (ICCES'05); 2005. p. 2522–7.

[37] Dongare AM, Neurock M, Zhigilei LV. Angular-dependent embedded atom method potential for atomistic simulations of metal–covalent systems. Phys Rev B, submitted for publication.

[38] Yu W, Wang ZQ, Stroud D. Empirical molecular dynamics study of diffusion in liquid semiconductors. Phys Rev B 1996;54:13946–54.

[39] Stephenson PCL, Radny MW, Smith PV. A modified Stillinger–Weber potential for modeling silicon surfaces. Surf Sci 1996;366:177–84.

[40] Balamane H, Halicioglu T, Tiller WA. Comparative study of silicon empirical interatomic potentials. Phys Rev B 1992;46:2250–79.

[41] Nakayama T, Itaya S, Murayama D. Nano-scale view of atom intermixing at metal/semiconductor interfaces. J Phys Conf Ser 2006;38:216–9.

[42] Predel B. In: Madelung O, editor. Landolt–Börnstein, group IV physical chemistry. Phase equilibria, crystallographic and thermodynamic data of binary alloys, vol. 5. Berlin: Springer-Verlag; 1991.

[43] Frenkel D, Smit B. Understanding molecular simulation. 2nd ed. San Diego and London: Academic Press; 2002.

[44] Kofke DA, Glandt ED. Monte Carlo simulation of multicomponent equilibria in a semigrand canonical ensemble. Mol Phys 1988;64:1105–31.

[45] Lin Z, Zhigilei LV. Time-resolved diffraction profiles and atomic dynamics in short pulse laser induced structural transformations: molecular dynamics study. Phys Rev B 2006;73:184113.

[46] Brandes EA, editor. Smithell's metal reference book. 6th ed. London: Butterworths; 1983.